Kepler: A Search for Terrestrial Planets

K2 Handbook

KSCI-19116-001

18 September 2017

Jeffrey Van Cleve
Steve Bryson

Table of Contents

Prepared by: _____ Date 9/15/2017
Jeffrey Van Cleve, Science Office

Approved by: _____ Date 9/19/2017
Doug Caldwell, Instrument Scientist

Approved by: _____ Date 9/15/2017
Jeffrey L. Coughlin, Science Office Director

Approved by: _____ Date 9/19/2017
Jessie Dotson, Project Scientist

3

1. Introduction to the K2 Handbook

The *Kepler* spacecraft was repurposed for the *K2* mission a year after the failure of the second of *Kepler*'s four reaction wheels in 2013 May. The purpose of this document, the K2 Handbook (K2H), is to describe features of *K2* operations, performance, data analysis, and archive products which are common to most *K2* campaigns, but different in degree or kind from the corresponding features of the *Kepler* mission.

1.1. Scope and Companion Documents

The K2H is meant to be read with these companion documents. Items 1-4 are retrievable from the MAST-Kepler web site, item 5 from the MAST-K2 web site, and item 6 from the *K2* science web sites:

1. *Kepler* Instrument Handbook (KSCI-19033) or KIH (Van Cleve and Caldwell, 2016), which provides information about the design, performance, and operational constraints of the instrument, and an overview of the types of pixel data that are available. With the exception of failed reaction wheels and CCD modules, the flight hardware for the *K2* mission is the same as that for *Kepler*, although the performance is quite different because of the roll.
2. *Kepler* Data Processing Handbook (KSCI-19081) or KDPH (Jenkins *et al.*, 2017). The KDPH describes how pixels downlinked from the spacecraft are converted by the *Kepler* Data Processing Pipeline (henceforth just "the pipeline") into the data products delivered to the MAST archive.
3. *Kepler* Archive Manual (KDMC-10008) or KAM (Thompson *et al.*, 2016). The KAM describes the format and content of the data products, and how to search for them.
4. *Kepler* Data Characteristics Handbook (KSCI-19040) or KDCH (Van Cleve et al., 2016). The KDCH describes recurring non-astrophysical features of the *Kepler* data due to instrument signatures, spacecraft events, or solar activity, and explains how these characteristics are handled by the final *Kepler* pipeline.
5. The Ecliptic Plane Input Catalog (EPIC) document (Huber and Bryson, 2017). The EPIC doc describes the provenance of the positions and *Kepler* magnitudes used for target management and aperture photometry, and is generally updated every 3 to 6 months. Stellar properties (mass, radius, log g, temperature, etc.) for *K2* targets are described in Huber *et al.* (2016) and made available by MAST as campaigns complete.
6. *K2* Data Release Notes (DRNs), which are on-line documents updated as appropriate, describe the data inventory, instrumental signatures, and events peculiar to individual campaigns, and the pipeline software changes between data releases. While K2H repeats some information in the DRNs, the K2H aggregates that information to show trends and ensure that crucial information applicable to multiple *K2* campaigns is not tied to a particular DRN.

The *Kepler* documents (items 1-4 above) will not be revised or reissued to accomodate *K2.* Instead, all K2-specific information will be bundled into the K2H. The authors, dates, and version numbers of the *Kepler* documents were updated at the end of the original *Kepler* mission, while the EPIC and DRNs will continue to evolve throughout *K2*. Acronyms are spelled out in the appendix of this document. This initial release of the K2H covers science data through the end of Campaign 13, operations through the end of Campaign 14, and flight planning through Campaign 15.

Several published papers provide more thorough treatments of *K2* flight operations (McCalmont et al., 2015), data analysis (Smith et al., 2016), and performance (Howell et al., 2014; Van Cleve et al., 2016) through roughly the first 1.5 years of science operations. The K2H will refer to these papers, but will not substantially reproduce their content.

1.2. Mission Timeline to Date

Figure 1: *K2* **mission timeline showing campaign boundaries and various historical events. The +VV fields are shown in lavender.**

K2 is constrained to point in the orbital plane, which is near the ecliptic (§2.1.2) and turns roughly 81 degrees every 83 days or so to view a new field of view (FOV) for a new observing campaign (denoted C<n> for n = 1 to 19). Typically, the telescope points away from the Earth ('anti-velocity vector' or –VV), but for synoptic viewing from Earth some campaigns (C9, C16, C17, and C19) point towards the Earth ('positive velocity vector' or +VV). *K2* has experienced the same kinds of science-interrupting events as *Kepler*, with comparable frequency. Thus the mission timeline (Figure 1) resembles that of *Kepler*. One qualitatively new event was a spacecraft Emergency Mode (EM) in April 2016, in which the Solid State Recorder (SSR) was powered off, but since we were between campaigns, no science data was actually lost. There were no EMs during the *Kepler* mission.

The data for C9-C11 was processed in two parts per campaign, for various reasons. C9 was split to accommodate a larger data volume for this microlensing campaign; most of the target resources were used to tile superapertures. C10 had an initial pointing error of more than 3 pixels in boresight, as a result of a miscommunication among the flight planning team. This error was corrected after 6 days, and the same set of apertures used throughout both parts of the campaign since the apertures were designed using the correct pointing. In addition, the correctly-pointed part of C10 is itself split by an unusually long gap during which module 4 failed and the spacecraft went into safe mode, though all the correctly-pointed data was processed together. In C11, there was a sign error in the YORP-related roll angle adjustment (§2.1.5). The correct sign changed the roll angle by 0.32^o = 40 science pixels, invalidating the designed apertures, and it took 3 weeks to notice the problem, diagnose it, and uplink new apertures. C1 and C2 had small pointing adjustments a few days after start of science, but not large enough to invalidate the photometric apertures. C0 and C1 had mid-campaign breaks, but the data were processed as a single campaign.

Campaigns in which data processing was split into two parts are designated a/b in some contexts and n1/n2 in others, where n is the campaign number. For example, 10b and 102 refer to the same data set. Alert users will notice the possibility of naming degeneracies in the numerical scheme, which fortunately have yet to manifest themselves.

1.3. Dates and Cadence Numbers

Cadences are defined in KDCH §1.1. The duration of long and short cadences are the same as they were in *Kepler*. Table 1 summarizes the start and end times and cadence numbers, which may also be

found in the individual DRNs. Campaigns which were split for various reasons have both alphanumeric and strictly numerical labels; for example, the 2nd half of campaign 9 may be referred to as 9b or 92 depending on context.

Table 1: Dates and Cadence Numbers through the end of C13. Start = beginning of first cadence, End = end of last cadence. 11b corrected a roll angle error in 11a.

Campaign	Start	End	LC Start	LC End	SC Start	SC End
0	12-Mar-2014 00:18:30	27-May-2014 16:48:13	87434	91186	2611480	2724069
1	30-May-2014 15:54:44	20-Aug-2014 20:19:37	91332	95353	2728420	2849079
2	23-Aug-2014 18:27:16	10-Nov-2014 13:27:43	95497	99352	2853370	2969049
3	15-Nov-2014 14:06:05	23-Jan-2015 18:37:04	99599	107213	2976430	3078009
4	08-Feb-2015 06:50:09	20-Apr-2015 04:32:47	103744	107213	2976430	3078009
5	27-Apr-2015 02:18:11	10-Jul-2015 22:39:43	107552	111214	3215020	3324909
6	13-Jul-2015 22:45:04	30-Sep-2015 21:11:29	111362	115224	3329320	3445209
7	04-Oct-2015 17:52:39	26-Dec-2015 08:35:28	115414	119456	3450880	3572169
8	04-Jan-2016 13:16:25	23-Mar-2016 06:48:35	119907	123759	3585670	3701259
9a/91	22-Apr-2016 14:04:59	18-May-2016 22:42:26	125243	126532	3745750	3784449
9b/92	22-May-2016 14:58:45	02-Jul-2016 22:34:52	126713	128734	3789850	3850509
10a/101	06-Jul-2016 19:45:29	13-Jul-2016 01:19:55	128925	129230	3856210	3865389
10b/102*	13-Jul-2016 01:49:21	20-Sep-2016 04:52:03	129231	132614	3865390	3966909
11a	24-Sep-2016 19:12:30	18-Oct-2016 02:16:19	132839	133979	3973630	4007859
11b	21-Oct-2016 06:17:05	07-Dec-2016 23:23:03	134134	136469	4012480	4082559
12	15-Dec-2016 20:40:49	04-Mar-2017 18:37:47	136855	140716	4094110	4209969
13	08-Mar-2017 01:35:06	27-May-2017 15:44:53	140878	144821	4214800	4333119

*Gap within this data set between cadences 129584 and 130268 inclusive

1.4. FFIs

These Full-Field Images (FFIs) were collected in *K2* through the end of C13:

```
ktwo2014070234206-c00_ffi-cal.fits
ktwo2014074233223-c00_ffi-cal.fits
ktwo2014110010101-c00_ffi-cal.fits
ktwo2014157010055-c01_ffi-cal.fits
ktwo2014203150825-c01_ffi-cal.fits
ktwo2014240042843-c02_ffi-cal.fits
ktwo2014294030900-c02_ffi-cal.fits
ktwo2014331202630-c03_ffi-cal.fits
ktwo2015008010551-c03_ffi-cal.fits
ktwo2015051131033-c04_ffi-cal.fits
ktwo2015092174954-c04_ffi-cal.fits
ktwo2015127093352-c05_ffi-cal.fits
ktwo2015170131810-c05_ffi-cal.fits
ktwo2015207050529-c06_ffi-cal.fits
ktwo2015246104018-c06_ffi-cal.fits
ktwo2015290001304-c07_ffi-cal.fits
ktwo2015331045232-c07_ffi-cal.fits
ktwo2016014203204-c08_ffi-cal.fits
ktwo2016056011138-c08_ffi-cal.fits
ktwo2016119231109-c91_ffi-cal.fits
ktwo2016153221424-c92_ffi-cal.fits
```

```
ktwo2016199030108-c102_ffi-cal.fits
ktwo2016240074042-c102_ffi-cal.fits
ktwo2016279022810-c111_ffi-cal.fits
ktwo2016307123729-c112_ffi-cal.fits
ktwo2016361035629-c12_ffi-cal.fits
ktwo2017032102633-c12_ffi-cal.fits
ktwo2017079075530-c13_ffi-cal.fits
```

The file names show the integration stop time in [year][3 digit day of year][hhmmss] format, followed by the campaign number. The FFIs have the same integration parameters as an LC exposure (~29.4 min), as was the case in *Kepler*. Note that only one FFI was collected in C13 in order to have enough storage for all the cadence data.

2. What's New in *K2*

2.1. Spacecraft and Instrument

2.1.1. Reaction wheel failures

The *Kepler* spacecraft lost the ability to precisely control its attitude while pointing at its target field in Cygnus when the 2nd of 4 reaction wheels failed in May 2013 (KDCH §4.7), leading to the qualitatively different attitude control and FOV scheme for *K2*.

2.1.2. Quasi-stable Attitude Control for Ecliptic Fields of View

The engineering solution to the loss of full 3-axis control is described in the papers by the Ball Aerospace engineers who developed it (Putnam, Gravseth, & Wiemer 2016; McCalmont et al. 2015; Peterson et al. 2015) and discussed colloquially in Van Cleve et al. 2016. In a nutshell, since solar radiation pressure is the main perturbing torque and the spacecraft is symmetric around the solar panel ridge, the roll axis is in unstable equilibrium when the boresight is pointed in the orbital plane (approximately the ecliptic). Residual torques then cause the spacecraft to roll, and the roll error is corrected with thruster firings every 6 hours or multiple thereof. The pointing performance is shown in **Table 3.**

2.1.3. Mod 7 and 4 failures

Module 3 failed during the *Kepler* mission, and module 7 failed between the *Kepler* and *K2* missions. Module 4 failed during C10b. Happily, there are 18 remaining science modules, and the current loss rate of a module every few years is not a mission-limiting factor. See KIH §4 for the arrangement of modules and other detector properties.

2.1.4. Attitude Determination and Control System (ADCS) Modifications

Star trackers, Fine Guidance Sensor (FGS) CCDs in the *Kepler* focal plane, reaction wheels, thrusters, and the ADCS software work together to acquire the desired attitude and keep the boresight at the commanded position in the face of solar radiation torques and thermomechanical drift between spacecraft and photometer components in the course of a campaign. McCalmont et al. (2015) give a detailed account of how these components had to be modified in *K2* to restore precise control of the boresight and acceptable control of spacecraft roll. To summarize from a user point of view:

1. There is only one guide star per module in *K2*, instead of the ten per module in *Kepler*. These are carefully screened to exclude variability > 10%, close companions, extended emission, and imposter galaxies. In some cases, suitable stars are so sparse that the availability of at least one guide star per module determines the FOV.
2. The control bandwidth was increased from 0.02 Hz to 0.05 Hz prior to campaign 3, greatly improving stability on SC time scales. During *Kepler*, it was 0.1 Hz.
3. The rate at which the spacecraft rolls about the boresight is inversely proportional to the angular momentum and hence wheel speed. The wheels are at their maximum speed immediately after thrusters are fired to unload angular momentum ("resats").
4. There are no longer reaction-wheel zero (speed) crossings (KDCH §5.4).

2.1.5. Coupling of Low Gain Antenna Operation to Roll Performance

Torques generated by the thermal emission of spacecraft equipment – the equivalent of the Yarkovsky-O'Keefe-Radzievskii-Paddack (YORP) effect on asteroids (Rubincam, 2000) – are an important part of *K2*'s angular momentum budget. Switching electronics boxes on or off will shift the equilibrium orientation of the spacecraft with respect to that determined in the *K2* engineering phase, with default power settings. The most salient example resulted from switching Low Gain Antennas (LGAs) in C7 (C7 DRN). LGA 1 was used for C0-C6, as in the *K2* engineering operations, but since the antenna gain is slightly better for LGA2 in the –VV direction the LGA was switched to #2 in C7 to compensate for signal loss as the *Kepler* spacecraft drifts away from Earth. C7 showed anomalously high roll error, which was diagnosed as a YORP effect, and the LGA was switched back to #1 shortly after the beginning of C8 to restore torques to

their expected values. LGA1 was used for the remainder of C8, C9, and C10. A change in roll angle was calculated to offset the YORP change and implemented in C11 for LGA2 operations. Unfortunately, the calculated sign of the change was wrong and C11 apertures had to be redefined in the middle of the campaign using the correct roll angle. Nominal roll torques with LGA2 operations were achieved for the latter part of C11 and C12-C13, with a return to LGA1 planned for C16 since it is a +VV orientation.

2.1.6. Motion-induced Invalid Cosmic Ray Correction

The cosmic ray (CR) detection and correction algorithm (KDPH §6.3.1) was developed using the observed characteristics of *Kepler* data. The design assumes wide-sense stationary data, for which the mean is constant and autocorrelation depends only on the time separation between points. *K2* data is not wide-sense stationary, since autocorrelation is time dependent (i.e., correlation between data points separated by a fixed time interval changes with absolute time due to roll cycle). Roughly speaking, motion-induced changes in flux on a given pixel can be mistaken for signal discontinuities produced by cosmic rays. This was recognized early in the mission, and CR detection and correction were turned off for target pixels for all of *K2*. However, CR detection was enabled for the collateral data, and generated many false positive detections in the smear and virtual smear as bright star flux shifted from column to adjacent column with image motion and generated outliers in the time series of the smear data. If the false positive CR is removed from the collateral data, then subtracting that collateral data gives spurious vertical bright streaks in the science data. Rather than turn off CR detection for collateral data, which would lead to a comparable amount of error from uncorrected CRs, it was found that an increase in the CR threshold would substantially reduce the number of false positives in the smear and virtual smear while continuing to do an adequate job of detecting real CRs. This higher threshold was used in C11 and subsequent campaigns and reprocessing.

CR detection and correction was used on background pixels throughout the *K2* mission, since these apertures were designed not to contain significant stellar flux, and hence are relatively insensitive to image motion induced flux discontinuities.

2.2. Target Management

2.2.1. Overview: Monotony to Diversity

The *Kepler* mission looked at the same field in Cygnus for 4 years. The boresight was fixed, and the spacecraft rolled 90 degrees each quarter. Almost all targets and guides stars were thus simply transferred from one CCD to another for the entire mission, and while targets of special interest were added or especially uninteresting stars were removed, the target list was by and large the same throughout the mission. Targets were selected before launch from a stable *Kepler* Input Catalog (KIC), except for a small GO (Guest Observer) program. A set of optimal aperture (OA) pixels were calculated for each target, and the OA fit by the best mask selected from a finite set of masks using the TAD (Target Aperture Definition) software described by Bryson et al. (2010a, 2010b) and KDPH §3. A key function called by TAD is raDec2Pix, which converts the target's astrometric RA and DEC to module, output, row, and column locations in the focal plane using the focal plane models (KAM §2.3.5) and the spacecraft boresight RA, DEC, and commanded roll angle. raDec2Pix does *not* include the roll error about the boresight that is a normal part of *K2* operations.

In contrast, the *K2* mission requires a new round of target management for every campaign, including selection of a FOV, selection of targets within that FOV, and the selection of aperture pixels corresponding to those targets. Targets are selected from an Ecliptic Plane Input Catalog (EPIC) which expands to include each new FOV (Huber and Bryson 2017). In addition, *K2* includes qualitatively new types of targets, such as Solar System Objects (SSOs), which were entirely unforeseen when *Kepler* was designed.

The strategy adopted to balance the need for code stability with the ever-changing needs of *K2* was to have a stable core of pipeline programs for target and aperture definitions (TAD, KDPH §3) with flexible MATLAB programs to create the input for TAD, examine its outputs, trim the target list to fit the pixel

budget given the estimated compression, and create summary reports for evaluation and approval by the Science and Guest Observer offices.

While no two *K2* campaigns are exactly the same, the work flow more-or-less follows this order:

1. The FOV is finalized after rough consideration of science targets and detailed consideration of the availability of FGS guide stars. While the RA and DEC of the FOV center is constrained to be in the ecliptic, and the roll angle is set by the stability requirement, the FOV center can be shifted in ecliptic longitude to maximize a science merit function while having at least one suitable guide star on each FOV module.
2. The updated EPIC is delivered and science targets selected through the GO proposal processs.
3. GO delivers stellar target lists, galaxy radii, bright stars with custom circular apertures, SSOs, and overrides to catalog values for proper motion and magnitude. The "stellar" targets are targets for which TAD defines the aperture and may include galaxies as well as stars.
4. Masks and apertures are designed for custom targets (§2.2.4 - §2.2.6). The set of pixels requested for a single physical target may be broken down into multiple smaller apertures, each of which has a custom EPIC ID assigned to it, in order to conserve space in the mask table. Generally, custom target apertures are "perfect" in that no excess pixels are requested, because the required target pixels are used to define the associated mask.
5. TAD is run to define apertures and masks for non-custom targets (stars and small galaxies). The masks are statistically optimized, though some targets – especially bright targets – will have excess pixels since the wide variety of optimal apertures cannot be perfectly fit by the finite number of masks and total number of mask pixels available, which includes the custom target mask set.
6. Compression estimates (§3.3) give the number of pixels available for LC and SC.
7. The LC and SC quasi-stellar lists are trimmed to meet the pixel budget, and the final quasi-stellar apertures calculated. In rare instances, custom targets are removed from the list.

2.2.2. KIC and EPIC Numbers

Kepler and *K2* use complementary target numbering schemes, collectively referred to as "*Kepler* Id," which include KIC, EPIC, and custom target numbers. KIC numbers were used only in *Kepler*, and have values $<10^8$. The relatively infrequent custom targets in the *Kepler* mission have *Kepler* Ids between 10^8 and $< 2.0 \times 10^8$ (KAM §2.2.1).

In *K2*, targets in the EPIC catalog have *Kepler* IDs $\geq 2.0 \times 10^8$ and $< 2.01 \times 10^8$ are assigned by TAD to custom targets when TAD is run, and it is expected the *K2* mission will end before this finite custom target ID space is exhausted. The same custom astronomical object may have multiple custom *Kepler* IDs, and will have different *Kepler* Ids for LC and SC observations, if both types of data are collected. For SSOs and sky regions, these numbers are sequential for a given target and may collectively be found in MAST by searching on the custom target name. EPIC numbers $\geq 2.01 \times 10^8$ indicate stars or galaxies that are actually in the EPIC with RA, DEC, and K_p, and which have had their apertures defined by TAD rather than the custom design process. Some small fraction of EPIC objects were selected for observation by *K2* and included in the *Kepler* Target Catalog (KTC), while all EPIC objects are used by TAD to model the sky and calculate optimal apertures. There is a continuing effort to supply stellar properties such as radius, temperature, and log g for those EPIC objects that were actually observed by *K2* (Huber et al., 2017).

The EPIC document's Table 0 shows EPIC IDs by campaign through C16. Some late targets are missing from C13-C16, and will be filled in as they become known. Note: The C9 comprehensive catalog originally had duplicate entries with C7. These duplicates have been removed without reassigning EPIC IDs. Therefore the number of targets in the comprehensive C9 catalog does not match the difference in EPIC IDs between the starting and ending EPIC ID.

2.2.3. Extra halos for Stellar Targets

In the *Kepler* mission, a "halo" of extra pixels was wrapped around the set of optimal aperture pixels in order to account for errors in catalog position, proper motion, and the small amount of image motion due to differential velocity aberration (<0.6 pixels) as attitude errors were negligible (KDPH §3). During *K2* C0, the roll errors were known to be at least a few pixels, and a conservative 10 halos were used, greatly increasing the number of pixels per target and therefore significantly decreasing the number of targets for which data could be stored. This was particularly severe for fainter stars; for example, the faintest *Kepler* star has a single-pixel optimal aperture giving a target aperture of 4x3 = 12 pixels, including one halo and one undershoot (KIH §6.6) correction column. In C0, this target would consume 22x21 = 462 pixels, a factor of 38 increase!

As *K2* progressed, understanding and control of the flight dynamics improved, and the maximum expected roll motion decreased, so that the number of halos decreased to 6 in C1, 3-4 in C2-C4, and 2-3 in C5 onward. The halos are smaller in the center of the FOV (less than 3.4 degrees from the center) since the roll motion is proportional to the distance from the FOV center for a given spacecraft roll error. Now, the smallest *K2* aperture is 6x5 = 30 pixels in the inner FOV and 8x7 = 56 pixels in the outer FOV.

The *K2* apertures are sized to collect all the pixels that might be in the optimal aperture throughout the campaign; in any particular cadence, some of the target pixels may not contain useful source flux. In the pipeline, a data-driven optimal aperture is calculated and used for all cadences (COA program, KDPH §7). While COA works well in a pipeline application which strives to be agnostic of scientific content, individual users may find that apertures which move or even change shape from cadence to cadence might be best for their particular science.

There are no halos on custom targets.

2.2.4. Solar System Objects (SSOs)

Kepler was never conceived to observe Solar System Objects (SSOs), but these are common targets in *K2*. Since these objects move, while apertures are defined for the entire campaign, the target pixels comprise an arc several pixels wide, which can traverse multiple channels. Defining a mask to cover an arc is impractical, since the mask could contain several thousand pixels per arc, and would be good only for that particular SSO since each arc has a different shape. The mask pixel budget of 87040 pixels would be quickly exhausted on SSOs alone, before attempting to fit the stellar targets! The solution was to define individual 'tiles' which together cover the arc; each tile is a custom target containing a single column (vertical) or a single row (horizontal) of pixels. The SSO pixels are then specified in a target list input file (TLIF), in which each target is a tile. Each SSO has its own TLIF. SSO arcs can be composed of a mix of horizontal and vertical tiles.

The path in astrometric RA and DEC of all SSOs are computed from JPL Horizons, for which the observer body ID of the *Kepler* spacecraft is -227 (in Horizons, spacecraft are assigned negative body ID numbers). K_p may be approximated from the Horizons visual magnitude, or from the literature. raDec2Pix then generates the SSO path (blue circles in Figure 2). Since the OA for stellar sources with $K_p \geq 15$ is a 2x2 box or smaller depending on the pixel response function (PRF) and subpixel registration, for faint SSOs the target pixels are "spraypainted" on the focal plane by convolving the path with a disk with default radius of 3.5 pixels (resulting in the yellow dots in Figure 2), which ensures the optimal pixels stay within the aperture even as *K2* rolls. Horizontal and vertical tiles are then assigned to exactly cover the target pixels, and the unique set of generated masks are inserted in the mask table.

For SSOs of intermediate brightness—bright enough to have optimal apertures larger than the faint stellar source limit, but not bright enough to bleed charge ($11.5 < K_p < 15$)—the target is treated as a series of instantaneous targets in a special Calculate Optimal Apertures (COA) run. The maximum width of the time union of optimal pixels is estimated and a convolution disk of that diameter used in the faint-source procedure. For example, this was done for Enceladus ($K_p \sim 12.3$) in C11b, for which the convolution disk radius was 5 pixels.

For the brightest SSOs ($K_p < 11.5$), the special COA run results are used directly, and a set of vertical or horizontal tiles defined to exactly cover the time union of OA pixels. The corresponding unique masks are inserted in the mask table. For example, this was done for Titan ($K_p \sim 8.9$) in C11b.

Use of the tiling scheme for SC SSOs can impose high data volume costs since the SC collateral (SCC) data is individually collected for each target (KIH 2.6.3.2), with no removal of duplications, and the uncompressed data volume of each SCC pixel time series is 30 times that of a LC pixel time series. For long arcs, the preferred scheme is then to cover the time union of OA pixels with a two-dimensional dedicated mask for a small number of targets (instead of one target per row/column). Duplication of SCC data is then reduced, but the mask table must accommodate a large dedicated mask, consuming mask table pixels that could be used to more efficiently cover the stellar targets. For example, in C8 the path of Uranus was tiled with 245 single column target definitions at long cadence but with eight 9 x 307 trapezoidal masks (and one small end cap mask) at short cadence. These masks eliminate the redundancy of SCC smear data, but there is still 8x redundancy in the SCC black data.

Data for a particular SSO may be easily located, either by family or individual names, on the MAST *K2* page by clicking on the "Object Type" button.
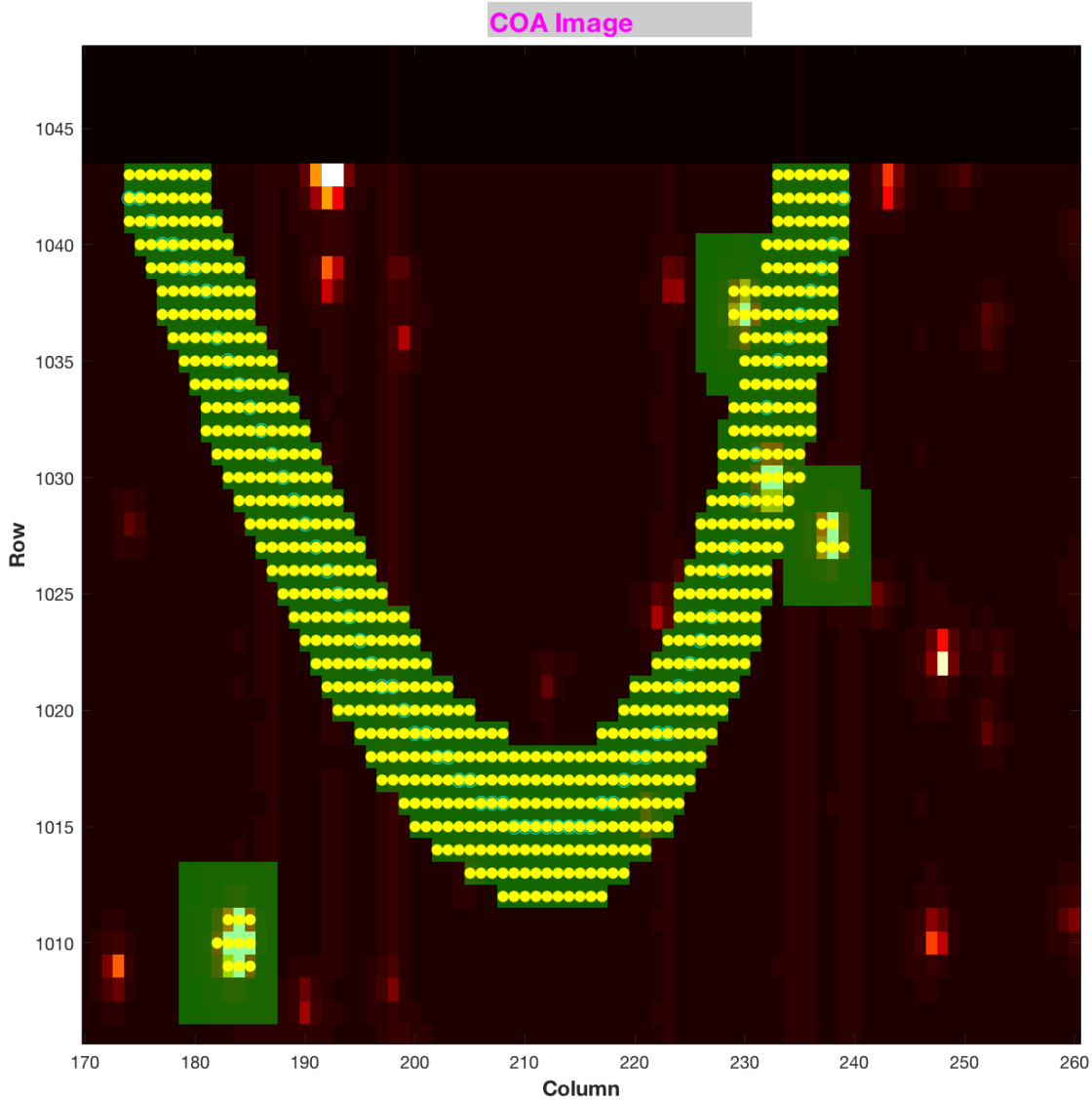
Figure 2: Example Dim ($K_p \sim 19.8$) SSO 2000_UX34 (Trojan). Blue circles show the custom targets comprising the path of the SSO, yellow dots the optimal aperture pixels, green = target pixels, red/white = stars. Roughly rectangular apertures near the arc, which do not contain a blue circle, are stellar targets.

2.2.5. Bright Stars

TAD optimal apertures for bright stars ($K_p < 6$) can be exceedingly large as charge bleeds across the array, since the TAD algorithm expects that good photometry cannot be done unless all the bleeding charge is captured in the optimal aperture. Furthermore, the statistical mask design process aims for efficient results only for stars with $K_p > 9$, so the large bright star apertures are not efficiently fit, compounding the pixel consumption. A 6th magnitude star, for example, typically has an aperture containing 4000 pixels, of which ~25% are excess – not in the optimal aperture, but in the target aperture because of the limitation of the finite mask set available. To remedy this problem, many bright stars are given custom apertures – a fixed disk of 24 to 40 pixels diameter, centered on the star. The photometry is done by modeling the wings of the PSF, with satisfactory results (Pope et al., 2017).

13

2.2.6. Galaxies

For extended emission from galaxies less than 40 arcsec in radius, the targets are listed in the EPIC and the stellar target list as if they were stars with an effective point source magnitude, but are given extra halos (but no undershoot columns) to capture the additional emission. For galaxies of > 40 arcsec diameter, a custom disk of fixed radius is defined since > 10 halos (masks ~25 pixels maximum linear dimension) may lead to inefficient mask selection in TAD.

2.2.7. Sky Regions

Science observation can be directed at an extended region of sky instead of an individual target, to look for unpredictable events such as gravitational lenses or supernovae, or to cover rich and complex areas like star clusters. If the area of the sky exceeds the typical aperture dimensions in the K_p range for which TAD generates efficient mask sets ($K_p > 9$, corresponding to masks ~25 pixels maximum linear dimension), the region is covered with smaller tiles. Examples include the superapertures for the gravitational lensing observations in C9, in which the 5 superapertures were assembled from 1748 custom target tiles, and the stellar clusters in C11.

2.2.8. Reduced Number of Nontarget Science Pixels

Because of the lower pixel budget in *K2* compared to *Kepler*, the Artifact Removal Pixels (ARPs, Van Cleve 2008) have been made spatially sparser starting in C2; C0 and C1 had a full set. There are 1174 ARP pixels per channel in *K2*, compared to 3355 in *Kepler*. The number of background pixels was also reduced after C0.

No reverse-clock (KIH §5.1) pixels (RC) were collected in *K2*.

2.3. Data Processing

Users should refer to the KDPH for a comprehensive description of the *Kepler* pipeline. Most of the important differences in data processing between *Kepler* and *K2* data, including corrected LC light curves, are described in DRN 5 (C3). Since then, some bugs and nonoptimal parameter values have been found and corrected: scrambled SCC data has been corrected, the threshold for LCC CR correction (§2.1.6) has been increased from 4 to 7, and a bug in the ordering of masked and virtual smear uncertainties (Propagation of Uncertainties, or POU) has been corrected. **Table 2** shows the processing status for these improvements.

Table 2: Data Processing Status as of 9/7/2017. Green = bug fixed in released data. Orange = bug not fixed in released data. Gray = data not yet released.

C	Latest Data Release #			Bug/param fix status				
	LC TPF	LC LC	SC TPF	SCC	LCC CR	SCC CR	LCC POU	SCC POU
0	2	n/a	2					
1	14	14	14					
2	4	4	4					
3	5	5	10					
4	6	6	10					
5	7	7	10					
6	8	8	8					
7	9	9	9					
8	11	11	11					
9	12	12	12					
10	15	15	15					
11	17	17	17					
12	18	18	18					
13	19	19	19					

2.4. Archive Files

The *K2* archive at MAST has the same types of files and file formats as Kepler (KAM §2.3), with three exceptions: there are no SC light curves or RC files, and there is new type of target pixel file, "Type-1." In general, file names have changed from `kplr*.fits` to `ktwo*.fits`, and minor changes to the headers (such as removal of the SEASON keyword and changing QUARTER to CAMPAIGN and MISSION to *K2*) have occurred.

In the early days of *K2*, calibrated target pixels were released while developing in parallel the software needed to produce light curves under *K2* conditions, rather than holding data release until the upgraded light curve software was ready to be run in its entirety. These target pixel files (TPFs) are called "Type-1 TPFs." Type-1 TPFs have WCS based on the ra_dec_2_pix focal plane model (KAM §2.3.5.14-16) and commanded pointing, rather than using a reconstructed pointing history. We expect that the Type-1 WCS coordinates can be off by 1-2 pixels given the unmodeled roll motion and discrete pointing offsets (§3.1). See §3.4 for an independent assessment of WCS fidelity.

In C3 and most subsequent *K2* processing, later stages of the pipeline are used to reconstruct the pointing history and associate thruster firings with specific long- and short-cadence numbers. That information is included in the TPFs, which are called "Type-2 TPFs." The standard Type-2 TPFs are part of all data releases which produce light curves, and contain WCS coordinates based on the reconstructed pointing, aberration, and local optical distortion determined from the measured PRF centroid motion of a number of bright unsaturated stars across each channel. This "motion polynomial" model (KDPH; Van Cleve, 2010 (KADN-26285)) tracks the roll drift and any impulsive pointing offsets, resulting in reconstructed position errors at or below 0.1 pixel for each cadence. Just as in *Kepler*, the FITS header reports only the WCS derived from the motion polynomials for the middle cadence of the campaign, so users of *K2* data will have to use the POS_CORR centroid offsets from the corresponding light curve file

to offset the WCS for individual cadence *K2* target pixel images in the Type-2 pixel files. Background is also subtracted in Type-2 TPFs, whereas it was not in Type-1 TPFs.

Type-1 TPFs were produced for C9, since most pixels were in superapertures and few stars with individual apertures were available for calculating motion polynomials. Type-1 TPFs were also produced for C10a, since the pointing error at the start of the campaign was large enough to invalidate the assigned photometric apertures.

Since the thruster firing flags are not populated in FITS quality flags for the Type-1 TPFs, they are being delivered in separate long-cadence and short-cadence thruster firing tables referenced in individual DRNs.

3. Evaluation of Performance

3.1. Pointing

Pointing stability in the *Kepler* mission was typically measured in 10's of millipixels, while that of *K2* is measured in pixels. The metric used to quantify pointing performance is the maximum distance between the derived and nominal positions for any target (the "maximum attitude residual", or MAR) calculated by the pipeline Photometer Performance Assessment (PPA) Attitude Determination (PAD) module (see KDPH). MAR is presented as a time series for several campaigns in the DRN, while a statistical summary through C12 is shown in **Table 3.** MAR includes the initial constant pointing error as well as motion throughout the campaign; roughly speaking, the 10th percentile MAR is the constant part and the difference between 10th and 90th percentile quantifies the motion.

Table 3: Maximum Attitude Residual in science pixels over time. The 90th percentile MAR is noticeably worse in C7 than the other campaigns, while in C13 ~2% percent of cadences were afflicted by anomalous thruster firings, as discussed in detail in the C7 and C13 DRNs. C0 and C9 do not have MAR statistics since light curves were not generated for those campaigns and the PPA-PAD module was therefore not run. Gapped data are excluded from these statistics.

C	10th p	median	90th p	99th p	max
1	0.25	0.61	1.13	1.55	1.92
2	0.22	0.58	1.16	1.63	2.15
3	0.28	0.58	1.10	1.68	2.06
4	0.19	0.49	0.96	1.41	1.99
5	0.38	0.77	1.27	1.61	1.86
6	0.33	0.60	1.15	1.63	2.12
7	0.25	0.92	1.84	2.65	3.37
8	0.27	0.64	1.25	1.74	2.29
10	0.41	0.70	1.16	1.51	1.69
11.1	0.50	0.96	1.48	1.95	2.19
11.2	0.39	0.90	1.50	1.84	2.13
12	0.31	0.67	1.17	1.65	3.17
13	0.34	0.66	1.18	1.88	3.26

3.2. CDPP for Pipeline Light Curves

Combined Differential Photometric Precision (CDPP) is the effective noise in the transit detection process (Jenkins et al., 2010). In addition to instrumental factors, CDPP depends on the duration of the transit, the magnitude of the star, and the star's intrinsic variability. The natural benchmark CDPP for *Kepler* and *K2* is a 6 h transit of a 12th magnitude dwarf (log g > 4.0) star and we will maintain this benchmark throughout this document unless explicitly referencing other durations, magnitudes, or stellar types when quoting CDPP. While CDPP is in general a function of time, here we discuss only the median or rms average over a time series for a given star; the default is rms average. These per-star values can then be further summarized as percentiles over stars for a given output channel or for the FOV as a whole; for example, $CDPP_{10}$ is the 10th percentile of CDPP over all stars. Simpler noise metrics, such as a Savitsky-Golay filter (Van Cleve et al., 2016) or running standard deviation such as KEPSTDDEV (see GO software page[1]), can be used to approximate CDPP. **Table 4** shows CDPP vs. two important factors

---

[1] https://*Kepler*science.arc.nasa.gov/software.html

which can degrade light curve quality: the motion component of MAR (90th-10th percentile), and the presence of bright ($K_p <= 6$) planets in the FOV.

Van Cleve et al. (2016) examined pipeline light curves for C3-C6 and found that $CDPP_{10}$ increases linearly with distance from the FOV center, in proportion to roll motion, while the $CDPP_{10}$ at the center of the FOV – where roll motion is least – is 30 ppm, only 25% higher than that for *Kepler*.

Each DRN contains scatter plots and FOV images of CDPP, and a link to a table showing 10th percentile and median CDPP over the FOV, sorted by magnitude bin.

C10b per-star CDPPs had to be calculated using medians over time, instead of an rms average, since the Presearch Data Conditioning (PDC) pipeline module (see the KDPH) which was used in all other campaigns for the CDPP calculation does not produce a meaningful number in the presence of large data gaps, such as that caused by the failure of mod 4 in C10b.

Table 4: 12th magnitude temporal rms average CDPP for dwarf stars vs. MAR variability and bright planets. C10b result is for temporal median since mod 4 failure gap in data made other metrics unavailable.

C	MAR(pix) 10th-90th p	CDPP (ppm) 10th p	CDPP (ppm) median	Bright planets
1	0.88	44.8	95.3	
2	0.94	71.2	128.7	Mars
3	0.82	44.2	94.8	
4	0.77	48.4	97.2	
5	0.89	40.2	75.2	
6	0.82	42.2	78.7	
7	1.58	59.2	122.3	
8	0.98	47.0	96.2	Uranus
10b	0.74	43.8	111.6	
11.1	0.98	50.6	131.8	
11.2	1.11	58.5	125.6	Saturn
12	0.86	55.5	127.3	Mars
13	0.84	54.8	128.9	

3.3. Compression

Data compression is an essential feature of both *Kepler* and *K2* missions since data storage and downlink bandwidth are limited by the size of the on-board Solid State Recorder (SSR) and the Earth-*Kepler* distance, which by 8/1/17 was 0.96 AU. As succinctly stated in the KDCH, "The data compression scheme involves three steps: 1) requantizing the data so that the quantization noise is approximately a fixed fraction of the intrinsic measurement uncertainty (which is dominated by shot noise for bright pixels), 2) taking the difference between each re-quantized pixel value and a baseline value that was updated once per day, and 3) entropic encoding via a length-limited Huffman table (Jenkins & Dunnuck, 2011)".

As noted in Van Cleve *et al.* (2016), *K2* data contains more (not necessarily interesting) information than *Kepler* data because of image motion and the high star count in some regions of the sky viewed by *K2*. More information increases the number of bits per pixel (denoted as *B* in subsequent discussion) needed to represent the data without significant compression losses, and requires that collection of *K2* baselines

every 12 h instead of 24 h. The *Kepler B* was between 4.6 and 5.4 bits per pixel without significant dependence on position in the FOV or star count. In contrast, the *K2 B* increases roughly linearly with radial distance from the FOV center (as does roll motion), and as the square root of star count n* until n* reaches the Olbers-Barclay limit, above which *B* is insensitive to n* (Figure 3). The Olbers-Barclay limit is roughly 1.2×10^4 stars per square degree for $11.5 < K_p < 14.5$, and conjectures (Barclay, 2016, private communication) that the sky as sampled by *Kepler*'s 4.0 arcsec pixels is becoming more uniform, not less, as n* increases beyond the O-B limit. The maximum contribution of n* to *B* is then 5.0 bits per pixel, and the maximum *B* for *K2* data with in-family roll errors is ~15 bits per pixel. Hence, it is always beneficial to compress the 16-bit requantized data (steps 2 and 3 above). In regions of low n*, such as the Galactic caps, the average *B* over the FOV is roughly 7.2 bits per pixel after the introduction of new Huffman table in C5 which is a better match to the distribution of data values in K2.
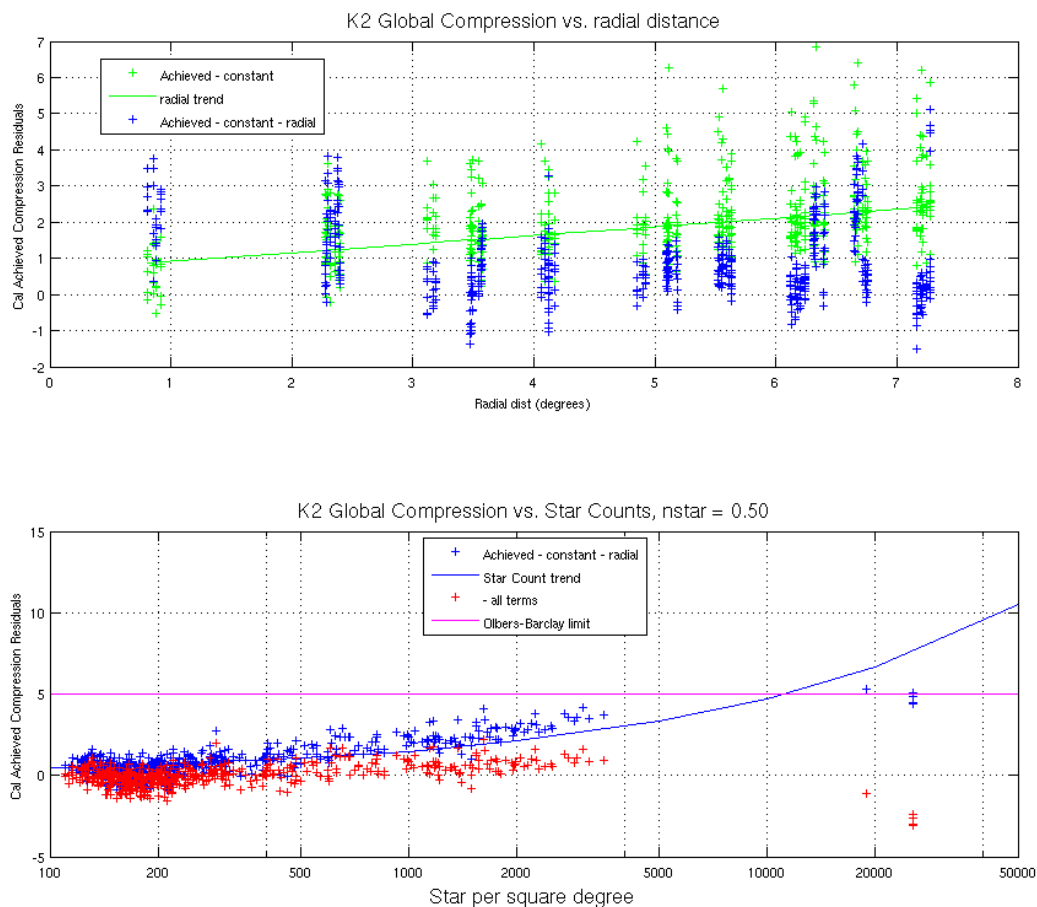

Figure 3 : Global Trends in *K2* Compression *B* in bits per pixel. Upper Panel: Data and fit vs. radial distance from FOV center. Lower Panel: Residual from constant + radial fit vs. count of 11 < K_p < 14.5 stars (n*). The solid blue line is the sqrt(n*) term obtained by fitting data with n* < 4×10^3 stars/deg^2, while the points (from C9) on the right show that for n* > 1.2×10^4 *B* no longer increases with n*, and may even decrease as n* increases.

3.4. Fidelity of World Coordinate System (WCS)

Handberg and Lund (2017) did an independent study of the fidelity of the *K2* WCS for both Type-1 and Type-2 TPFs. They found that the absolute correction in pixels to the estimated position of targets, based

on the WCS provided in target pixel files, was a function of angular distance to the FOV center (see Figure 6 of Handberg and Lund, 2017). For the Type-1 data, with a model-derived WCS, corrections could be as large as 1.0 pixels, while for Type-2 data (C3 and C4) the maximum correction was 0.5 pixels with typical corrections ~0.2 pixels. They conclude, for Type-2 data, "…this level of off-set should in general be small enough to correctly identify targets in the frames." Lund et al. (2016) Figure 9 shows graphically the correction of the WCS pixel positions in C0 Type-1 data.

Custom non-point targets also have WCS coordinates. Even though there may not be a well-defined point source in the aperture, a centroid is nonetheless calculated to set the reference location within each aperture (keywords CRPIX1, CRPIX2). While this position is arbitrary, the WCS transformation is derived from the motion polynomials (Van Cleve, 2010), which are calculated from good stars on that channel, not from the custom target itself, and the WCS keywords correctly describe the mapping of pixels to/from sky.

3.5. SSOs

Szabo et al. (2016) present example SSO photometry with $K2$ data, in this case for Trojan asteroids. The photometric precision required for SSOs is typically 0.1% - 1.0%, instead of the 100 ppm required for transits and asteroseismology; $K2$'s main strength for most SSOs is uninterrupted temporal coverage for up to 80 days rather than its raw photometric precision. In some ways, SSO photometry is easier (much of what follows in this section is from A. Pal, private communication):

1. Most SSOs are faint (K_p > 15) so shot noise is relatively more important than systematics, unlike for brighter objects.
2. Many $K2$ fields have lower star counts than the $Kepler$ field, reducing systematic noise from stars moving in and out of a synthetic aperture co-moving with the SSO.
3. The motion of the SSO in itself seems to reduce systematics, possibly because that motion is a form of natural dithering which averages out the intrapixel response nonuniformity which was an important part of the $Kepler$ error budget.

Some exceptions to this relative ease, for which systematic error removal is a research topic in itself, include:

1. Pluto, which is bright (K_p = 14.2), slow, and moves slowly across the Galactic plane.
2. Titan and Enceladus, which are contaminated by light from Saturn and its rings.
3. Neptune, for which global oscillations were sought with an upper limit of ~5 ppm at 1000 µHz (Rowe et al., 2017)
4. Uranus, which is bright (K_p ~ 6) and has four major satellites potentially in the aperture.

A 0- vs. 1-based indexing error in the SSO target definition algorithm was discovered in Sept. 2017, which afflicts all SSO data taken through the end of C15. The requested pixels are one pixel to the left and one pixel below their correct positions, in an image orientation with the origin in the lower left, row number as the ordinate, and column number as the abscissa. In the correct tile target sets, the object path should be centered in the union of target pixel tiles. The object path itself had the correct pixel coordinates, only the assignment of pixels was affected by the bug. While users may see this offset in movies of the object path (for example, the Pluto movie in the C7 DRN or other movies in http://tiny.cc/k2videos), they may not notice significant problems with photometry due to this bug since the tile sizing already included 2-3 pixels margin for roll error. The bug has been fixed in time for C16 target management. An example for Chiron in C12 is shown in Figure 4.
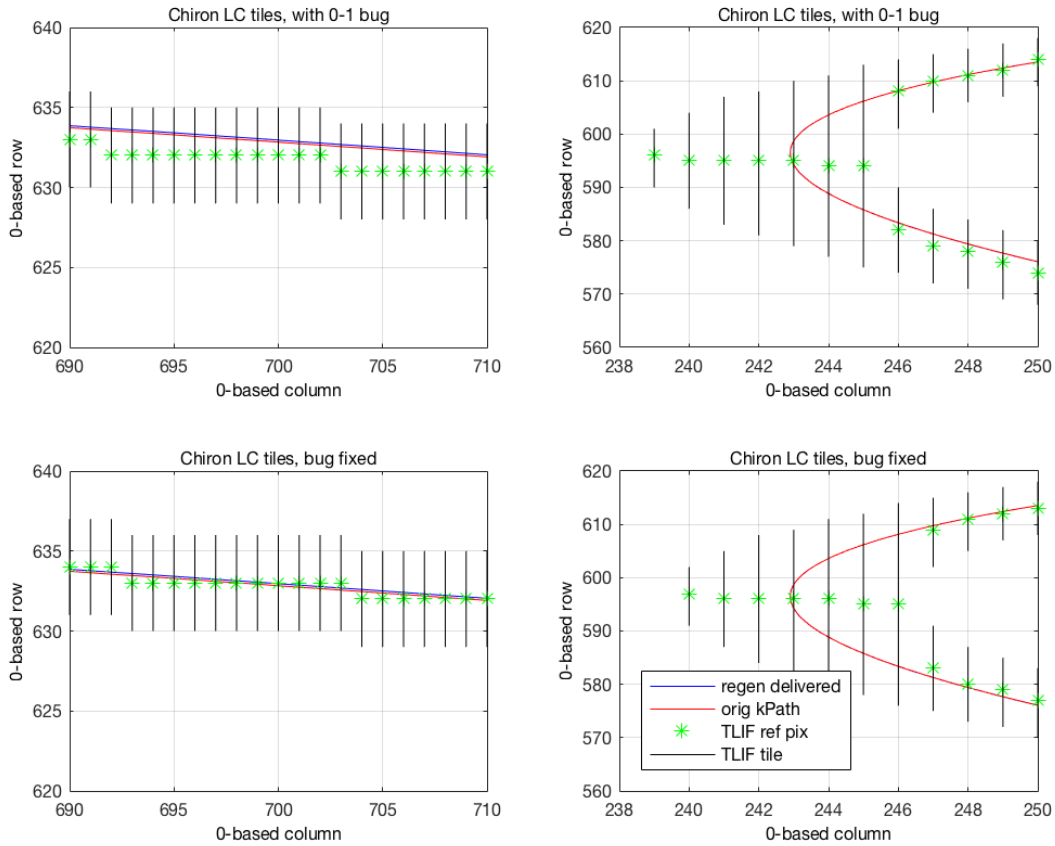
Figure 4: 0-1 base indexing error in SSO tiles, example for C12 Chiron LC observations. Upper panels: buggy tiles on straight path (left) and at ansa (right). Lower panels: tiles produced by corrected algorithm. The regenerated and original target paths are the blue and red lines, respectively, and show that the target path pixel coordinates were correctly calculated to better than 0.1 pixels.

3.6. FGS Guide Star Variability

FGS guide star variability affects photometry by causing pointing offsets. In C6, for example, false signals as large as 1000 ppm were impressed on light curves by the telescope motion induced by a variable guide star, as discussed in the C6 DRN and its more technical addendum[2]. Users wishing to investigate this topic further should see §4.3.

---

[2] https://keplerscience.arc.nasa.gov/images/release-notes/c6/var_fgs_kso-391_drnC6_addendum_16040722.pdf

4. Engineering Data

4.1. Two-wheel Concept Engineering Test Data (E2)

The year-long transition from *Kepler* to *K2* following the reaction wheel failures is detailed in Larson et al. (2014). Part of this transition was a 9-day engineering test (E2) conducted before Campaign 0. While E2 was not intended for science, the data have been made available as uncalibrated TPFs at MAST http://archive.stsci.edu/missions/k2/eng/. The E2 FOV overlaps with C12 to a large extent, so users might do their own reduction of E2 data for comparison to C12 observations to look for long-term trends in common objects. The E2 FOV was centered at (RA, DEC) = (358.5, -2.4).

The inventory files at MAST use non-standard KepIDs between 60017806 and 60044117. They are not in EPIC, so users will have to match the RA and DECs to some other suitable catalog.

4.2. Engineering Data for Science Campaigns

The same ancillary engineering data are available for *K2* as for *Kepler* (KIH §2.5; KAM §2.3.10 and Appendix B.5). Items of particular interest are the engineering telemetry which has changed significantly between *Kepler* and *K2*, such as the roll error ADATTERRMX and the various temperatures of subsystems which experience a different thermal environment in *K2* than in the *Kepler* mission. **Figure 5** shows an example.
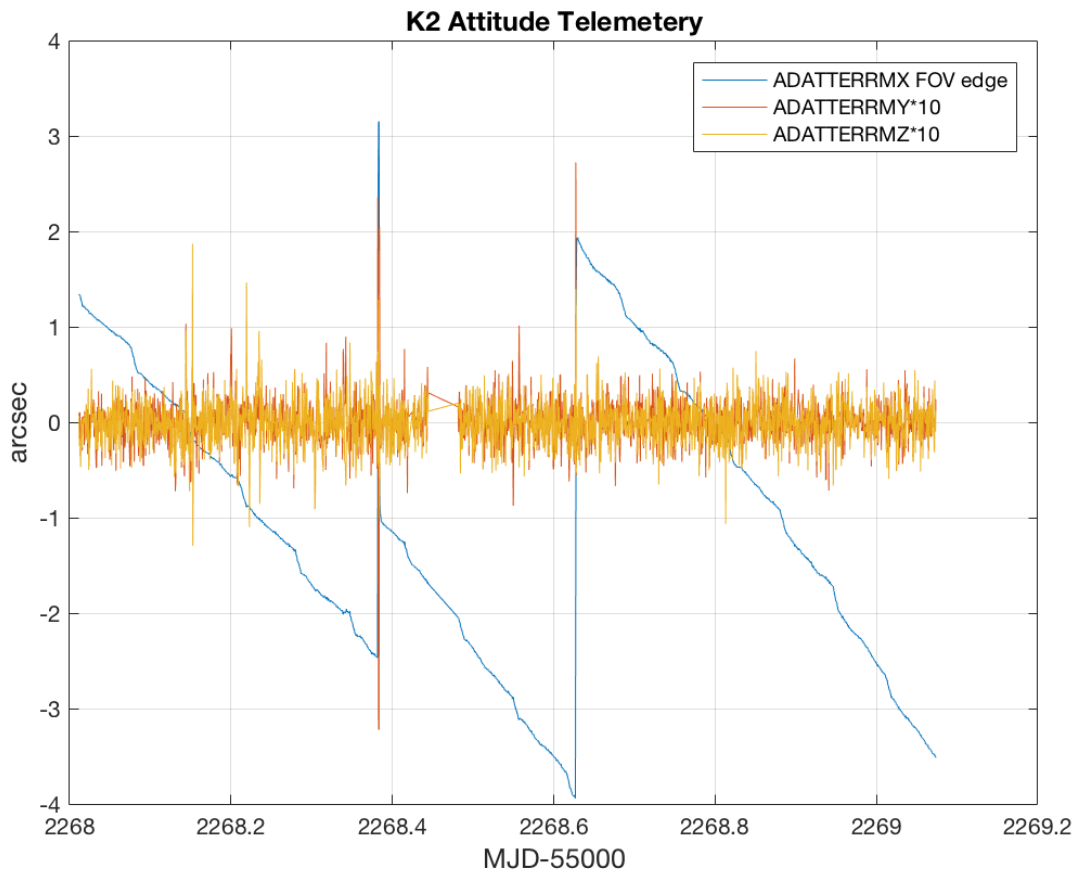

Figure 5: Example Engineering Telemetry from *K2*. ADATTERRMX is the roll about the boresight. It has been converted from radians to arcsec, and multiplied by the FOV radius in radians, to get the image motion in arcsec at the FOV edge.

22

4.3. FGS Data for Science Investigations

The FGS data are available at MAST for science investigations, in the form of centroid/flux time series and as (relatively infrequent) FGS FFIs. Users may find stellar variability or eclipsing binaries, or use the FGS data to more fully understand correlations and other properties of the science data. More information is available in the document KSCI-19112-001 (Van Cleve & Campbell, 2017).

5. References

Key Web Sites
https://archive.stsci.edu/*Kepler/* (MAST-*Kepler*)
http://archive.stsci.edu/k2/ (MAST-K2)
https://Keplerscience.arc.nasa.gov/index.html (K2)

Publications
Bryson, S. T., *et al.* 2010a, ApJL, 713, L97
Bryson, S. T., Jenkins, J. M., Klaus, T. C. *et al.* 2010b, Proc. SPIE, Vol. 7740, 77401D
Handberg, R., and Lund, M. N. 2017, A&A, 597, A36
Howell, S. B., Sobeck, C., Haas, M. R., *et al.* 2014, PASP, 126, 398
Huber, D., Bryson, S. T., Haas, M. R., et al. 2016, ApJ Supplement, 224, 2
Jenkins, J. M., *et al.* 2010a, ApJL, 713, L87
Jenkins, J. M., *et al.* 2010b, ApJL, 713, L120
Jenkins, J. M., Dunnuck, J. 2011, Proc. SPIE Vol. 8146, 814602
Larson, K. A., McCalmont, K. M., Peterson, C. A., and Ross, S. E. 2014, SpaceOps 2014 Conference, SpaceOps Conferences, (AIAA 2014-1882) http://dx.doi.org/10.2514/6.2014-1882
Lund, M. N., Handberg, R., Davies, G. R., Chaplin, W. J., Jones, C. D., 2015, ApJ, 806, 30L
McCalmont, K. M., Larson, K. A., Peterson, C. A., and Ross, S. E., 2015, AIAA SPACE 2015 Conference and Exposition, doi: 10.2514/6.2015-4530
Peterson, C. A., Larson, K. A., McCalmont, K. M., and Ross, S. E., 2015, AIAA SPACE 2015 Conference and Exposition, http://arc.aiaa.org/doi/abs/10.2514/6.2015-4534
Pope, B. J. S., White, T. R., Huber, D., *et al.* 2016, refereed (MNRAS.455L..36P)
Putnam, D., Gravseth, I., and Wiemer, D., 2106, AIAA Guidance, Navigation, and Control Conference (2016) doi: 10.2514/6.2016-0366
Rowe, J. F.; Gaulme, P.; Lissauer, J. J., et al. 2017, AJ 153:149
Rubincam, D. 2000, Icarus, 148, 2–11
Smith, J. C., Morris, R. L., Jenkins, J. M., Bryson, S. T., Caldwell, D. A., Girouard, F. R. 2016, PASP, 128:124501
Szabó, Gy. M., Pál, A., Kiss, Cs., et al. 2016, A&A 599 A44
Van Cleve, J. E., Howell, S. B., Smith, J. C., *et al.* 2016, PASP, 128:075002
Witteborn, F., Van Cleve, J. E., Borucki, W., and Argabright, V. 2011, Proc. SPIE, Vol. 8151, 815117

Kepler project documents available at MAST
Huber, D., and Bryson, S. T. 2017, KSCI-19082-014 "K2: Extending *Kepler*'s Power to the Ecliptic"
Jenkins, J. M., Caldwell, D. A., and Gilliland, R. L. 2004, KSOC-21008 "Algorithm Theoretical Basis Document" (ATBD)
Jenkins, J. M., *et al.* 2017, KSCI-19081-002 "*Kepler* Data Processing Handbook" (KDPH)
Thompson, S. E., Fraquelli, D., Van Cleve, J. E., and Caldwell, D. A. 2016, KDMC-10008-006 "*Kepler* Archive Manual" (KAM)
Van Cleve, J. E., 2008, KADN-26205 "Selection of LDE Artifact Removal Pixels for Science Operations and Reverse-Clock Calibration"
Van Cleve, J. E., 2010, KADN- 26285 "World Coordinate System for Target Pixel FITS Files Derived from Linearized Pipeline Motion Polynomials"
Van Cleve, J. E., and Caldwell, D. A. 2016, KSCI-19033-002, "*Kepler* Instrument Handbook" (KIH)
Van Cleve, J. E. *et al.* 2016, KSCI-19040-005 "Kepler Data Characteristics Handbook" (KDCH)
Van Cleve, J. E., and Campbell, J. 2017, KSCI-19112-001, "Fine Guidance Sensor Data"

Appendix A. List of Acronyms

ADCS   Attitude Determination and Control Subsystem
AED   Ancillary Engineering Data
BATC   Ball Aerospace & Technologies Corp.
BJD   Barycentric Julian Date
BKJD   Barycentric *Kepler* Julian Date
CAL   Calibration (pipeline software)
CBV   Cotrending Basis Vector
CCD   Charge Coupled Device
CDPP   Combined Differential Photometric Precision
COA   Calculate Optimal Aperture (pipeline module)
CR   Cosmic Ray
DAWG   Data Analysis Working Group
DV   Data Validation (pipeline software)
DVA   Differential Velocity Aberration
FFI   Full Field Image
FGS   Fine Guidance Sensor
FOV   Field of View
FPA   Focal Plane Assembly
GO   Guest Observer
HGA   High-Gain Antenna
JD   Julian Date
LC   Long Cadence
LDE   Local Detector Electronics
MAD   Median Absolute Deviation
MAST   Mikulski Archive for Space Telescopes
MJD   Modified Julian Date = JD - 2400000.5
PA   Photometric Analysis (pipeline software)
PAD   Photometer Attitude Determination (pipeline software)
PDC   Pre-search Data Conditioning (pipeline software)
PPA   Photometer Performance Assessment (pipeline software)
ppm   parts per million
PRF   Pixel Response Function
SC   Short Cadence
SNR   Signal-to-Noise Ratio
SO   Science Office
SOC   Science Operations Center
SSR   Solid-State Recorder
STScI   Space Telescope Science Institute SVD Singular Value Decomposition
TDB   Barycentric Dynamical Time
TPS   Transiting Planet Search (pipeline software)
UTC   Universal Time Coordinated
VTC   Vehicle Time Code